Journal of Orthopaedic Translation 42 (2023) 1–14

Contents lists available at ScienceDirect

Journal of Orthopaedic Translation

journal homepage: www.journals.elsevier.com/journal-of-orthopaedic-translation

Pharmacological inhibition of protein S-palmitoylation suppresses osteoclastogenesis and ameliorates ovariectomy-induced bone loss

Linghui Ma [a,b,1], Liwei Zhang [c,1], Zirui Liao [b,1], Chunmei Xiu [a,1], Xi Luo [b], Na Luo [b], Lei Zhang [b], Guangxu He [d,**], Jianquan Chen [a,b,*]

[a] Key Laboratory of Novel Targets and Drug Study for Neural Repair of Zhejiang Province, Department of Clinical Medicine, School of Medicine, Hangzhou City University, Hangzhou, Zhejiang, China
[b] Orthopedic Institute, Suzhou Medical College, Soochow University, Suzhou, Jiangsu, China
[c] Department of Orthopedics, Taizhou Hospital of Zhejiang Province, Zhejiang University, Taizhou, Zhejiang, China
[d] Department of Orthopedics, The Second Xiangya Hospital, Central South University, Changsha, Hunan, China

ARTICLE INFO

Keywords:
Protein S-palmitoylation
2-bromopalmitic acid
Osteoclastogenesis
Osteoporosis

ABSTRACT

Background: Excessive osteoclast formation disrupts bone homeostasis, thereby significantly contributing to pathological bone loss associated with a variety of diseases. Protein S-palmitoylation is a reversible post-translational lipid modification catalyzed by ZDHHC family of palmitoyl acyltransferases, which plays an important role in various physiological and pathological processes. However, the role of palmitoylation in osteoclastogenesis has never been explored. Consequently, it is unclear whether this process can be targeted to treat osteolytic bone diseases that are mainly caused by excessive osteoclast formation.

Materials and methods: In this study, we employed acyl-biotin exchange (ABE) assay to reveal protein S-palmitoylation in differentiating osteoclasts (OCs). We utilized 2-bromopalmitic acid (2-BP), a pharmacological inhibitor of protein S-palmitoylation, to inhibit protein palmitoylation in mouse bone marrow-derived macrophages (BMMs), and tested its effect on receptor activator of nuclear factor κβ ligand (RANKL)-induced osteoclast differentiation and activity by TRAP staining, phalloidin staining, qPCR analyses, and pit formation assays. We also evaluated the protective effect of 2-BP against estrogen deficiency-induced bone loss and bone resorption in ovariectomized (OVX) mice using μCT, H&E staining, TRAP staining, and ELISA assay. Furthermore, we performed western blot analyses to explore the molecular mechanism underlying the inhibitory effect of 2-BP on osteoclastogenesis.

Results: We found that many proteins were palmitoylated in differentiating OCs and that pharmacological inhibition of palmitoylation impeded RANKL-induced osteoclastogenesis, osteoclast-specific gene expression, F-actin ring formation and osteoclastic bone resorption *in vitro*, and to a lesser extent, osteoblast formation from MC3T3-E1 cells. Furthermore, we demonstrated that administration of 2-BP protected mice from ovariectomy-induced osteoporosis and bone resorption *in vivo*. Mechanistically, we showed that 2-BP treatment inhibited osteoclastogenesis partly by downregulating the expression of c-Fos and NFATc1 without overtly affecting RANKL-induced activation of osteoclastogenic AKT, MAPK, and NF-κB pathways.

Conclusion: Pharmacological inhibition of palmitoylation potently suppresses RANKL-mediated osteoclast differentiation *in vitro* and protects mice against OVX-induced osteoporosis *in vivo*. Mechanistically, palmitoylation regulates osteoclast differentiation partly by promoting the expression of c-Fos and NFATc1. Thus, palmitoylation

Abbreviations: ZDHHC, zinc finger aspartate-histidine-histidine-cysteine (DHHC) domain-containing enzyme; ABE, acyl-biotin exchange; 2-BP, 2-bromopalmitic acid; BMMs, bone marrow-derived macrophages; RANKL, receptor activator of nuclear factor κβ ligand; TRAP, tartrate-resistant acid phosphatase; μCT, micro-computed tomography; qPCR, quantitative real-time polymerase chain reaction; ELISA, enzyme-linked immunosorbent assay; OCs, osteoclasts; CCK-8, cell counting kit-8; M-CSF, macrophage-colony stimulation factor; α-MEM, α-minimum essential medium; DPBS, Dulbecco's PBS; P/S, penicillin/streptomycin; FBS, fetal bovine serum; RIPA, radioimmunoprecipitation assay; ALP, alkaline phosphatase; H&E, hematoxylin and eosin; CTX-1, carboxy-terminal cross-linked telopeptide of type 1 collagen; OCN, osteocalcin; EZH2, enhancer of zeste homologue 2.

* Corresponding author. 51 Huzhou Street, Gongshu District, Hangzhou, Zhejiang, 310015, China.
** Corresponding author.
E-mail addresses: heguangxu1987@csu.edu.cn (G. He), chenjq@hzcu.edu.cn (J. Chen).
[1] These authors contributed equally to this study

https://doi.org/10.1016/j.jot.2023.06.002
Received 8 May 2023; Received in revised form 16 June 2023; Accepted 28 June 2023

plays a key role in promoting osteoclast differentiation and activity, and could serve as a potential therapeutic target for the treatment of osteoporosis and other osteoclast-related diseases.

The translational potential of this article: The translation potential of this article is that we first revealed palmitoylation as a key mechanism regulating osteoclast differentiation, and therefore provided a potential therapeutic target for treating osteolytic bone diseases.

1. Introduction

Osteoclasts (OCs), the multinucleated giant cells, are differentiated from monocyte/macrophage cells of the hematopoietic lineage [1]. As the only known cell type that is specialized for bone resorption, OCs play pivotal roles in bone development, growth and homeostasis [1]. Moreover, aberrantly increased number and/or activity of OCs represent the main pathological cause of bone loss in a variety of skeletal diseases, such as osteoporosis, osteoarthritis, rheumatoid arthritis, periprosthetic osteolysis, periodontal disease, and bone metastasis of cancer [2–7]. Given these important physiological and pathological roles of OCs in the skeleton, great efforts have made in the past decades to dissect the molecular mechanism governing osteoclastogenesis. It is now well-accepted that osteoclastogenesis is dictated by two key signal molecules, i.e., macrophage-colony stimulation factor (M-CSF) and receptor activator of nuclear factor (NF)-κβ ligand (RANKL) [1,3,8]. These two factors induce osteoclast differentiation by activating multiple downstream signaling pathways including p38, ERK, JNK, NF-κβ and AKT pathways, and several key osteoclastogenic transcriptional factors such as c-Fos and NFATc1 [3,8,9]. Despite these progresses, our understanding of the mechanism regulating osteoclastogenesis is still incomplete.

Protein S-palmitoylation (hereafter abbreviated as palmitoylation) is a post-translational lipid modification involving the covalent linkage of the 16-carbon saturated fatty acid palmitate to free thiol groups of specific cysteine residues within target proteins through thioester bonds [10,11]. It is distinguished from all other forms of lipid modifications by its reversibility [10,12]. Specifically, palmitoylation is catalyzed by ZDHHC family of palmitoyl acyltransferases consisting of 23–24 members in mammals that all contain an aspartate-histidine-histidine-cysteine (DHHC) motif within a zinc finger-like domain, and can be reversibly removed by depalmitoylating enzymes such as PPT1, PPT2, APT1, APT2, ABHD17 A/B/C and ABHD10 [10–14]. Accumulating evidence indicates that palmitoylation occurs in a large variety of proteins, including some G proteins, signaling proteins, receptors, ion channels, transporters and kinases [15,16]. In fact, palmitoylated proteins are estimated to account for over 10% of proteome of human or other organisms studied thus far [17]. Palmitoylation regulates protein intracellular trafficking, subcellular localization, stability and activity as well as protein-protein interactions, thereby playing important roles in various physiological and pathological processes [10,11,16].

Several studies have indicated that palmitoylation is also involved in regulating bone homeostasis. A number of proteins were palmitoylated in differentiating osteoblasts, and pharmacological inhibition of palmitoylation hindered osteoblast differentiation and mineralization [18]. Consistent with these *in vitro* results, mice with *Zdhhc13* deficiency exhibited osteoporosis [19,20]. The further mechanistic study revealed that ZDHHC13 promoted bone formation in part by palmitoylating MT1-MMP [19]. In contrast to ZDHHC13, ZDHHC16 appears to negatively regulate osteogenic differentiation of mesenchymal stem cells by palmitoylation and subsequent inhibition of CREB [21]. Thus, palmitoylation could play a positive or negative role in osteoblastogenesis, depending on which ZDHHC is involved. In contrast to its role in osteoblast differentiation, the role of palmitoylation in osteoclastogenesis has never been explored. Consequently, it is unclear whether this process can be targeted to treat osteolytic bone diseases that are mainly caused by excessive osteoclast formation.

In this study, we utilized the pharmacological approach to explore the role of palmitoylation in osteoclast differentiation. We found that many proteins were palmitoylated in differentiating OCs, whereas 2-bromopalmitic acid (2-BP), a pharmacological inhibitor of palmitoylation, impeded RANKL-induced osteoclastogenesis *in vitro* and protected against ovariectomy-induced bone loss in mice. Mechanistically, we demonstrated that palmitoylation controlled osteoclast differentiation in part through modulating the c-Fos/NFATc1 expression. Thus, our findings demonstrated that palmitoylation is a key mechanism for promoting osteoclastogenesis, and that targeting this modification might serve as a novel therapeutic approach to treat osteolytic bone diseases.

2. Materials and methods

2.1. Antibodies and reagents

Rabbit primary antibodies for p38 (#8690), ERK (#4695), JNK (#9252), AKT (#9272), p-ERK (#4370), p-JNK (#4668), p-AKT (#9271), and NF-κB p65 (#8242) were purchased from Cell Signaling Technology (Danvers, MA, USA). Rabbit primary antibody for p-p65 (#11014) was obtained from Signalway Antibody (SAB) (Greenbelt, Maryland, USA). Rabbit anti-GAPDH antibody (GB11002) was obtained from Servicebio (Wuhan, Hubei, China). Rabbit antibodies specific for p-p38 (#ab4822), NFATc1 (#ab25916), and c-Fos (#ab190289) were purchased from Abcam (Waltham, MA, USA). All above primary antibodies were used at 1:2000 dilution in 5% BSA. HRP-linked goat anti-rabbit secondary antibody (#7074S) was provided by Cell Signaling Technology (Danvers, MA, USA), and used at 1:4000.

The α-minimum essential medium (α-MEM), and Dulbecco's PBS (DPBS) were from BasalMedia Technologies (Shanghai, China). Penicillin/streptomycin (P/S) and trypsin were obtained from NCM Biotech (Suzhou, Jiangsu, China). Fetal bovine serum (FBS, #FBS500-S) were from AusGeneX (Oxenford, Australia). Recombinant mouse macrophage-colony stimulating factor (M-CSF) (#CB34) and receptor activator for nuclear factor-κB ligand (RANKL) (#P00226) were purchased from Novoprotein (Suzhou, Jiangsu, China) and Solarbio (Beijing, China), respectively. 2-BP (#238422) was purchased from Sigma-Aldrich (St. Louis, MO, USA). Radioimmunoprecipitation assay (RIPA) lysis buffer, phosphatase inhibitor cocktail (#P1082), Prestained Color Protein Ladder (#P0078) Cell Counting Kit-8 (CCK-8, #C0039), 2% Alizarin Red S Staining Solution (#C0138**),** Alkaline Phosphatase Color Development Kit (#C3206), Alkaline Phosphatase Assay Kit (#P0321), phalloidin-FITC (#C1033), and 4,6-diamidino-2-phenylindole (DAPI) (#C1002) were all provided by Beyotime Biotechnology (Shanghai, China). Protease Inhibitor Cocktail (#K1007) were purchased from APExBIO (Houston, TX, USA).

2.2. Preparation of bone marrow-derived macrophages (BMMs)

Bone marrow macrophages (BMMs) were prepared from bone marrow cells isolated from tibiae and femurs of 8-10-week-old C57BL/6 mice following the protocol described below. Bone marrow cells in the femur and tibia of mice were isolated by pulse centrifugation, and plated in 10 cm cell culture dishes with α-MEM culture medium (α-MEM medium containing 10% FBS and 1% P/S). The next day, non-adherent cells were collected, re-plated in 10 cm cell culture dishes, and then cultured in BMM growth medium (α-MEM culture medium supplemented with 15 ng/ml recombinant mouse M-CSF) for 24 h. Afterwards, non-adherent cells were removed by rinsing the cultures three times with DPBS. The remaining adherent cells were considered as BMMs, and allowed to grow

in BMM growth medium for additional 2–3 days until they reached 80–90% confluency. BMMs were subsequently harvested by trypsinization and seeded in cell culture plates at the indicated density. All cell cultures were performed at 37 °C in a humidified incubator with 5% CO2 (v/v), and the medium was refreshed every 2 days.

2.3. Culture and osteoblastic induction of MC3T3-E1 cells

Mouse MC3T3-E1 cells were routinely maintained in α-MEM containing 10% FBS and 1% P/S (hereafter referred as α-MEM growth medium) at 37 °C in a humidified incubator with 5% CO_2 (v/v). To examine the effects of 2-BP on osteoblastic differentiation, MC3T3-E1 cells were seeded in cell culture plates at a density of $4 \times 10^4/cm^2$, and then induced with osteogenic medium (OM) consisting of α-MEM growth medium supplemented with 100 nM dexamethasone, 50 μg/ml ascorbic acid, and 10 mM β-glycerophosphate, in the presence of 0, 6.25, 12.5, or 25 μM of 2-BP for indicated days. The medium was refreshed every 2 days. At 7 days of osteoblastic induction, cells were subjected to alkaline phosphatase (ALP) staining, lysed for protein isolation and subsequent ALP activity assay, or harvested for RNA isolation and qPCR analysis. ALP staining and ALP activity assay were performed using Alkaline Phosphatase Color Development Kit(#C3206) and Alkaline Phosphatase Assay Kit (#P0321), respectively.

2.4. Cell Counting Kit-8 (CCK-8) assays

The cytotoxic effects of 2-BP on BMMs were determined by the CCK-8 assays as described previously [3]. Briefly, 5×10^3 BMMs were seeded in wells of 96-well plates and cultured overnight in BMM growth medium. The next day, the cells were treated with indicated concentrations of 2-BP for 24 h, 48 h or 72 h. At the specified time point, CCK-8 reagent (10 μl/well) was added to each well, and the plates were incubated at 37 °C for an additional 2 h. Finally, the absorbance at a wavelength of 450 nm (OD_{450}) was measured using the ELX800 absorbance microplate reader (BioTek, Winooski, USA).

2.5. In vitro osteoclastogenesis assays

In vitro osteoclastogenesis assays were carried as previously described (Zhang et al., 2020). Briefly, BMMs were inoculated in 24-well plates (for TRAP or F-actin ring staining) or 6-well plates (for RNA isolation) at a density of 1×10^5 or 4×10^5 cells per well, respectively. After overnight culture in BMM growth medium, BMMs were induced with osteoclastic medium in the presence of vehicle (DMSO) or different concentrations of 2-BP. The medium was refreshed every other day until formation of mature OCs in the vehicle-treated group (usually 5–6 days), and then cells were lysed for RNA isolation, or subjected to either TRAP or F-actin ring staining.

2.6. TRAP and F-actin ring staining

TRAP staining was performed as we previously described [3]. For F-actin ring staining, cells were fixed with 4% paraformaldehyde (PFA) for 10 min, followed by permeabilization with 0.1% Triton X-100 in DPBS for 5 min and then by incubation with 2.5% BSA in DPBS for 20 min. Afterwards, cells were stained with phalloidin-FITC (#C1033, Beyotime Biotechnology, 1:100 diluted in 2.5% BSA) for 1 h in the dark at RT. After washing with DPBS, the cells were counterstained with 4, 6-diamidino-2-phenylindole (DAPI) (#C1002, Beyotime Biotechnology, 1:2000 diluted in DPBS) for 5 min, rinsed again with DPBS, and then imaged with an inverted fluorescent microscope (Carl Zeiss Microscopy, Thornwood, NY). ImageJ software (National Institutes of Health, MD, USA) was used to quantify the number and relative length of F-actin rings as well as nuclei per osteoclast in each group. Three wells per group were analyzed.

2.7. Resorption pit assay

BMMs (8×10^3 cells/well) were seeded in a 96 well Corning Osteo Assay plate (#3988, Corning), and cultured overnight in BMM growth medium. The next day, the cells were treated with osteoclastic medium (OCM) combined with vehicle (DMSO) or different concentrations of 2-BP (6.25, 12.5, or 25 μM) for 5 d with medium replaced every other day. The plates were then bleached with 5% sodium hypochlorite for 5 min, washed twice with ddH2O, and air-dried. Afterwards, resorption pits on the plates were visualized using an inverted microscope (Carl Zeiss Microscopy, Thornwood, NY), and the percentage of resorption area out of the total plate area were determined with the ImageJ software (National Institutes of Health, MD, USA).

2.8. Quantitative real-time PCR (qPCR)

Total RNA was extracted from cells using RNA isolater Total RNA Extraction Reagent (#R401, Vazyme, Nanjing, China), and then reverse-transcribed into cDNA using HiScript III RT SuperMix (#R323, Vazyme). Quantitative real-time PCR (qPCR) was performed with above cDNA as the template using ChamQ Universal SYBR qPCR Master Mix (#Q711, Vazyme). The cycling conditions were 95 °C for 3 min, 40 cycles of 95 °C for 10 s and 60 °C for 30 s, followed by a melting curve stage (65 °C–95 °C, increment 0.5 °C, 5 s/cycle). Relative gene expression was calculated by the $2^{-\Delta\Delta Ct}$ approach with *18S* as an internal control. The primers used in this study were synthesized by Sangon Biotech (Shanghai, China), and their sequences were provided in Supplemental Table 1.

2.9. Western blot analysis

To investigate the effect of 2-BP on RANKL-induced activation of osteoclastic signaling pathways and protein expression, two separate sets of experiments were performed. In the first one, BMMs were seeded in 6-well plates at 6×10^5 cells per well, and cultured in BMM growth medium overnight. The next day, BMMs were pretreated with vehicle (DMSO) or 25 μM 2-BP for 4 h, and then stimulated with 100 ng/ml RANKL for 0, 5, 15, 30 or 60 min. In the second experiment, BMMs (4×10^5 per well) were inoculated and cultured as described above, followed by stimulation with osteoclastic medium in the presence of vehicle (DMSO) or 25 μM 2-BP for 0, 1, 3, and 5 days. At each time point of both experiments, total protein was extracted from cells using radioimmunoprecipitation assay (RIPA) lysis buffer containing protease and phosphatase inhibitors, and then analyzed by western blot as we previously described [3].

2.10. Acyl-biotin exchange (ABE) assay

For Acyl–biotin exchange (ABE) assays, BMMs were plated in 10 cm cell culture dishes (8–10 dishes for each group), and induced with osteoclastic medium for 3 days as described above. In case of 2-BP treatment, vehicle (DMSO) or 25 μM 2-BP was included in the osteoclastic medium. Cells from each 10 cm culture dish were fully lysed with 1 ml LB buffer (150 mM NaCl, 50 mM Tris–HCl pH 7.4, 5 mM EDTA pH 7.4) supplemented with 10 mM N-ethylmaleimide (NEM) (E3876, Sigma), 2 mM phenylmethanesulfonyl fluoride (PMSF) (#ST505, Beyotime Biotechnology), 2 × Protease Inhibitor Cocktail (PI) (#K1007, ApexBio), and 1.7% Triton X-100 (#T8787, Sigma). Afterwards, cell lysates from the same group were pooled and centrifuged at 4500 rpm for 10 min at 4 °C. The supernatants were collected and their protein concentrations were determined using a BCA Protein Assay Kit from Beyotime Biotechnology (Shanghai, China). Equal amounts of protein samples (5 mg/group) were precipitated with methanol-chloroform and incubated with SB buffer (4% SDS, 50 mM Tris–HCl pH7.4, 5 mM EDTA pH 7.4) containing 10 mM NEM at 37 °C for 10 min, followed by treatment with 3 mM NEM overnight to block free thiol groups. The next day, protein samples were precipitated with methanol-chloroform to remove free NEM, and

subsequently dissolved in SB buffer. Samples were then evenly divided into two halves (designated as + HA and -HA), which were respectively incubated with 2 mM HPDP-biotin (#21341, Thermo Scientific) in the presence or absence of 0.7 M hydroxylamine (HA) (#S30348, Yuanye Biotechnology) at RT for 1 h. Next, samples were precipitated and then treated with 0.2 mM HPDP-biotin at RT for additional 1 h, followed by removal of excess HPDP-biotin by methanol-chloroform precipitation. The protein pellets were then dissolved in LB buffer containing 0.2% Triton X-100, 1 mM PMSF, and 1 × PI. An aliquot (10% of protein sample) was taken and saved as the input control (Input). The remaining proteins in each group were incubated with streptavidin-agarose resin (#20349, Thermo Scientific) at RT for 1.5 h. Subsequently, beads were washed 4 times with LB buffer containing 0.1% SDS and 0.2% Triton X-100, and then collected by brief centrifugation. The pulldown proteins were eluted with LB buffer containing 0.1% SDS, 0.2% Triton X-100, and 1% β-mercaptoethanol. Finally, the input and pulldown protein samples from both + HA and -HA groups were resolved by SDS–PAGE and subjected to either coomassie blue staining or western blot analyses.

2.11. Animals and treatments

All animal studies were performed under the National Institutes of Health (NIH) Guide for the Care and Use of Laboratory Animals, and approved by the Ethics Committee of Soochow University and the Experimental Animal Welfare Ethics Committee of Hangzhou City University. Ovariectomy (OVX)-induced osteoporosis model was generated as previously reported [22]. Briefly, after being anesthetized with intraperitoneal injection of 50 mg/kg pentobarbital sodium, 10-week-old female C57BL/6 mice were bilaterally ovariectomized (OVX group) or subjected to resection of partial fat tissue adjacent to bilateral ovaries (Sham group). After 3 days of recovery from surgery, OVX mice were injected intraperitoneally with vehicle solution (5%DMSO, 30% PEG300 and 10% Tween-80) for the OVX group (n = 7), 2.5 mg/kg 2-BP in vehicle solution for the 2-BP-L group (n = 7), or 5 mg/kg 2-BP in vehicle solution for the 2-BP-H group (n = 7) once a day for 5 weeks. The high dose of 2-BP (5 mg/kg) was chosen based on a previous study that applied the same dosage of 2-BP to mice without causing any detrimental effect [23]. As the control, mice in the sham group (n = 7) were also treated with vehicle solution. At the end of treatment, the mice were sacrificed, the uteri were assessed to validate the OVX operation, the whole blood was drawn to obtain serum for enzyme-linked immunosorbent assay (ELISA), and the femurs were harvested for micro-computed tomography (μCT) and histological analyses.

2.12. Micro-computed tomography (μCT) and histological analyses

For μCT analysis, femurs were fixed in 10% neutral formalin for 2 d, and then washed three times with PBS. Afterwards, the fixed femurs were scanned and the obtained raw images were processed as we previously described [22]. Subsequently, trabecular bone parameters within the region of interest (ROI), including bone volume/tissue volume (BV/TV), trabecular thickness (Tb.Th), trabecular number (Tb.N), and trabecular separation (Tb.Sp), were determined using the CTAn software (Bruker, Aartselaar, Belgium). ROI was defined as the trabecular region of 100 μCT slices (about 0.9 mm in thickness) starting from 50 slices (about 0.45 mm) proximal to the distal growth plates of femurs. For histological analysis, femurs were decalcified, paraffin-embedded, sectioned, then subjected to hematoxylin and eosin (H&E) and TRAP staining as previously described [22].

2.13. Enzyme-linked immunosorbent assay (ELISA)

To determine the effect of 2-BP treatment on bone resorption and bone formation in mice, serum samples were prepared and levels of carboxy-terminal cross-linked telopeptide of type 1 collagen (CTX-1) and osteocalcin (OCN) in serum were subsequently evaluated as we previously described [22] using the CTX-1 (#E-EL-M3023) and OCN (#E-EL-M0864c) ELISA kits, respectively. Both kits were provided by Elabscience (Wuhan, Hubei, China).

2.14. Statistical analysis

Quantitative data were collected from at least three biological replicates, analyzed using GraphPad PRISM 8 (GraphPad Software, San Diego, CA), and finally presented as bar graphs or dot plots with means ± SD (standard deviation). Statistical differences between groups were determined by Student's t-test, one-way ANOVA with Tukey's post-hoc test, or two-way ANOVA with Sidak's post-hoc test as indicated in the figures. In all analyses, a value of $p < 0.05$ was considered as statistically significant, and levels of statistical significance were further marked in the graphs by numbers of asterisk (*): * for $p < 0.05$; ** for $p < 0.01$; *** for $p < 0.001$, and **** for $p < 0.0001$.

3. Results

3.1. Protein S-palmitoylation occurs in differentiating OCs

As the first step to investigate whether protein S-palmitoylation is involved in OCs differentiation, we examined its status in differentiating osteoclasts. Specifically, we harvested proteins from BMMs after 3 days of osteoclastic induction with RANKL, and then performed ABE assays on protein samples with or without hydroxylamine (HA) pretreatment. The purified proteins (labeled as Pulldown) as well as protein aliquots before the final streptavidin–agarose purification step (labeled as Input) were separated onto SDS-PAGE gels, and then stained with coomassie blue. As shown in Fig. 1A, a few bands were purified from the samples without HA pretreatment (-HA group). The most prominent band was at the molecular weight (MW) of about 70 kDa. In addition to these nonspecific bands, many more proteins with various sizes were specifically purified from HA-treated protein samples (+HA group), indicative of palmitoylated proteins. Most of these proteins had molecular weights in the range between about 45 and 120 kDa (Fig. 1A). Thus, these results clearly indicate that protein S-palmitoylation occurs in differentiating OCs.

To reveal potential ZDHHCs that are responsible for protein palmitoylation during OCs differentiation, we performed qPCR analysis to examine expression kinetics of all 24 *Zdhhc* genes in BMMs at 0, 2, 4, and 6 d after osteoclastic induction. The results showed that the transcripts of *Zdhhc19, Zdhhc22,* and *Zdhhc25* were barely detected in BMMs or differentiating OCs, whereas expression of the remaining 21 *Zdhhc* genes can be readily detected in these cells (Fig. 1B–F, Supplemental Fig. 1). Among them, the transcript levels of *Zdhhc* 1, 5, 8, 15, and 17 were obviously elevated in the differentiating OCs compared to BMMs (Fig. 1B–F), suggesting that these ZDHHCs might play a positive role in osteoclastogenesis.

3.2. Pharmacological inhibition of palmitoylation impeded RANKL-induced osteoclast differentiation and osteoclast-specific gene expression in vitro

To investigate the functional significance of protein S-palmitoylation in osteoclastogenesis, we utilized 2-BP, a pharmacological inhibitor of protein S-palmitoylation. We first evaluated the cytotoxicity effect of 2-BP on BMMs using CCK-8 assays. The results showed that 25 μM or lower concentrations of 2-BP did not cause any discernible effect on cell viability even after 72 h of treatment (Fig. 2A–C), whereas higher concentrations of 2-BP (50 and 100 μM) exhibited dose-dependent cytotoxicity to BMMs (Fig. 2A–C). We then confirmed the inhibitory effect of 2-BP on palmitoylation. To this end, we employed (ABE) assays to enrich palmitoylated proteins from total proteins harvested from BMMs treated with the highest non-toxic concentration of 2-BP (25 μM) or vehicle for 2 days, and then performed western blot analysis of input and enriched proteins. The results showed that palmitoylation of R-Ras, the protein

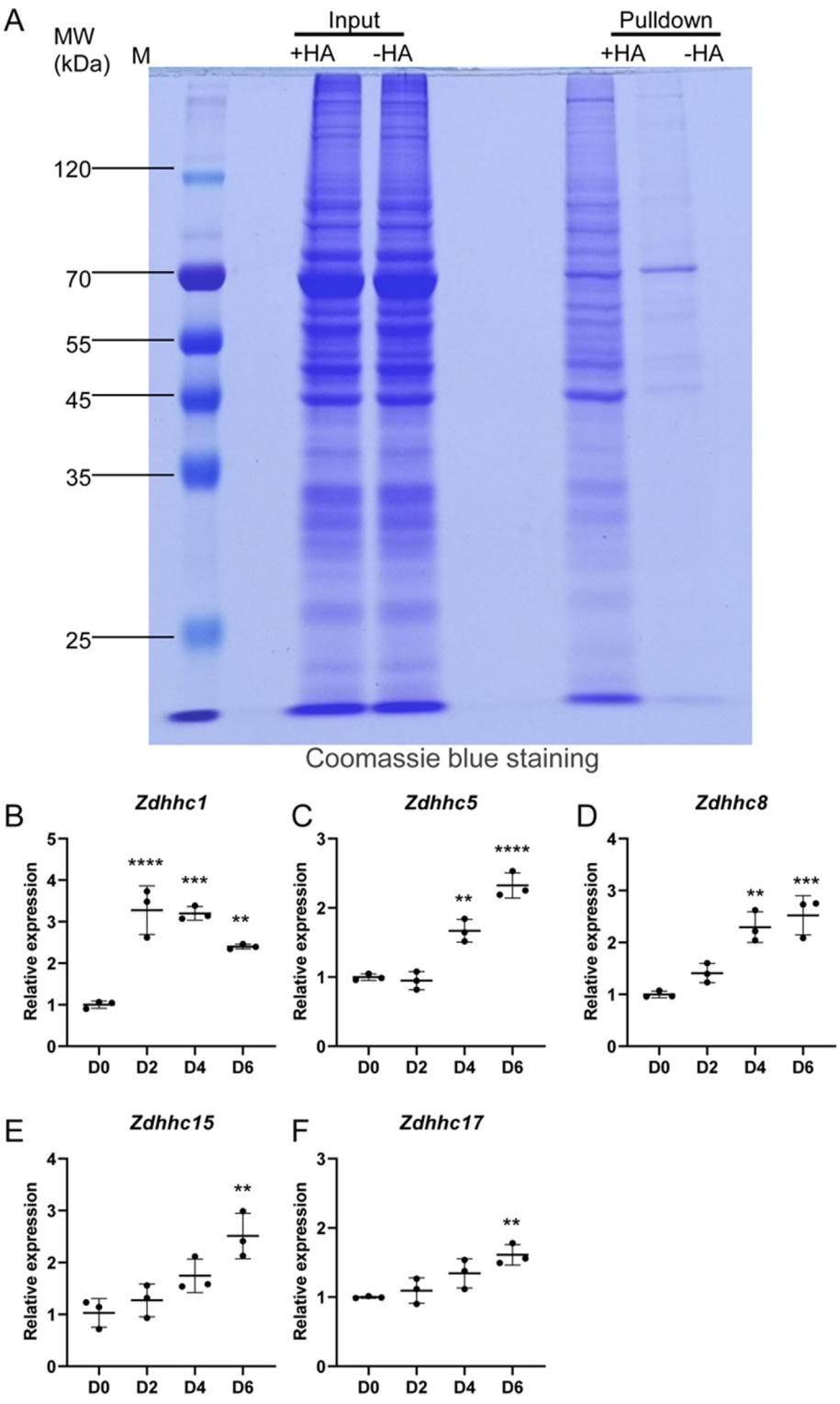

Fig. 1. Protein S-palmitoylation occurs in differentiating OCs. **(A)** Representative images of coomassie blue staining of protein samples before (Input) and after acyl-biotin exchange (ABE) assay (Pull-down). Total proteins were extracted from BMMs that were induced with 100 ng/ml RANKL for 3 days. Bands shown in the -HA lane of pulldown samples represented nonspecifically purified contaminant proteins. Additional bands in the +HA lane of pull-down samples indicated palmitoylated proteins. M, protein markers. Images shown were representative results from three independent experiments. **(B–F)** qPCR analysis of relative expression of *Zdhhc1* (B), *Zdhhc5* (C), *Zdhhc8* (D), *Zdhhc15* (E), *and Zdhhc17* (F) in BMMs before (D0) and after treatment with 100 ng/ml RANKL for 2 (D2), 4 (D4), and 6 days (D6). The relative changes in mRNA levels were analyzed by $2^{-\Delta\Delta CT}$ method. mRNA expression level of each target gene was first normalized to the expression of *18S* ribosomal RNA, and then normalized to the D0 group. n = 3 wells per group. All values were presented as mean ± SD. *p* values were determined by one-way ANOVA. *: $p < 0.05$, **: $p < 0.01$; ***: $p < 0.001$; ****: $p < 0.0001$, relative to D0 group.

that was known to be a substrate for palmitoylation [24,25], was severely impaired by 2-BP treatment (Fig. 2D), indicating that 2-BP can suppress protein palmitoylation in BMMs.

Next, we set to evaluate the effects of 2-BP on osteoclast formation *in vitro*. We induced BMMs for osteoclast differentiation in the presence of different concentrations of 2-BP (0, 3.125, 6.25,12.5, 25, or 50 μM) for 5 days. TRAP staining showed that numerous mature OCs, as characterized by TRAP-positive multinucleated cells with enlarged morphology, appeared in the RANKL-treated control group, whereas a notable reduction in mature OCs was observed in 2-BP-treated groups (Fig. 2E). This observation was further verified by quantitative analyses, which demonstrated that both number and size of mature OCs were dose-dependently reduced by 2-BP treatment (Fig. 2F and G). In addition to cellular morphological changes, RANKL-induced osteoclast differentiation is also accompanied by increased transcription of a set of osteoclast-related genes, such as *c-fos*, *Nfatc1*, *Ctsk*, *Acp5*, *Oscar*, *Dcstamp*, and

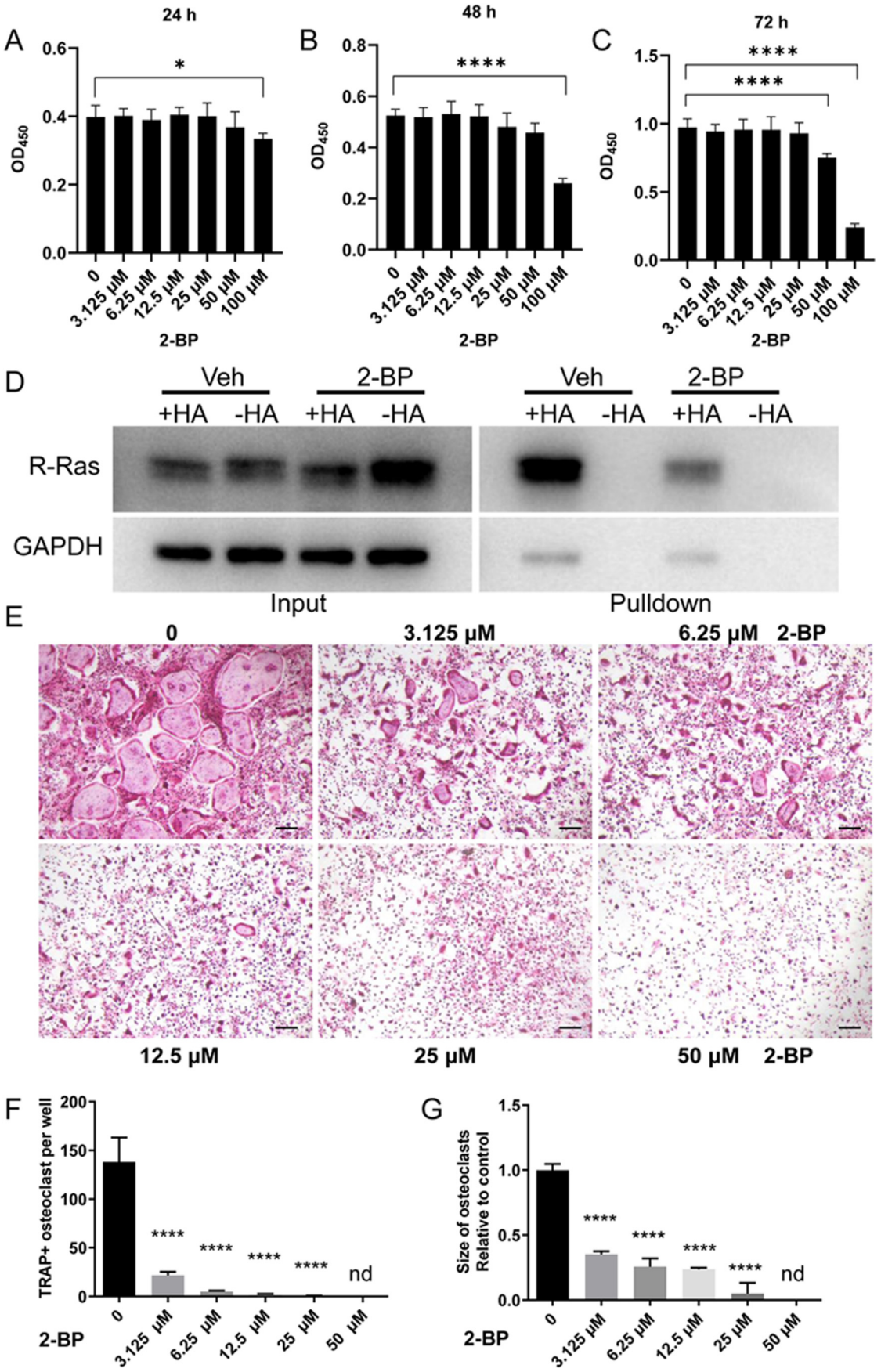

(caption on next page)

Fig. 2. 2-BP dose-dependently inhibited RANKL-induced osteoclast formation *in vitro*. (A–C) CCK-8 assays of BMM viability after they were treated with indicated concentrations of 2-BP for 24 (A), 48 (B), or 72 h (C). n = 6 wells per group**. (D)**. Palmitoylation of R-Ras was analyzed by ABE and western blot in BMMs treated with vehicle or 25 μM 2-BP for 2 days. Images shown were representative results from three independent experiments. **(E)** TRAP staining of BMMs after stimulation with 15 ng/ml M-CSF and 100 ng/ml RANKL in the presence of indicated concentrations of 2-BP for 5 days. Images shown were representative results from triplicates. Scale bar: 200 μm. **(F)** Quantification of average number of TRAP-positive multinucleated OCs per well. n = 3 wells per group. **(G)** Quantification of relative size of TRAP-positive multinucleated OCs. n = 3 wells per group. All values were presented as mean ± SD. *p* values were determined by one-way ANOVA. *: $p < 0.05$, **: $p < 0.01$; ***: $p < 0.001$; ****: $p < 0.0001$, relative to vehicle-treated group. nd, not detected.

Atp6v0d2. To further confirm the critical role of protein palmitoylation in osteoclastogenesis, we therefore performed qPCR analysis to examine the effect of 2-BP on the mRNA expression of these osteoclast marker genes, and found that their mRNA levels were all dose-dependently down-regulated by 2-BP treatment (Fig. 3).

Collectively, these data demonstrated that protein palmitoylation is critical for osteoclast differentiation, and pharmacological inhibition of protein palmitoylation in BMMs by 2-BP can dose-dependently suppress RANKL-induced osteoclast formation *in vitro*.

3.3. Pharmacological inhibition of palmitoylation suppressed RANKL-induced F-actin ring formation and osteoclastic bone resorption in vitro

To investigate whether 2-BP affects osteoclastic bone resorption, we first evaluated the effect of 2-BP on RANKL-induced formation of F-actin ring, an integral component of the cytoskeleton in mature OCs that is essential for their bone resorption activity. Analyses of phalloidin-stained cell cultures revealed that the number of cells forming typical F-actin rings was decreased by 2-BP in the dose-dependent manner (Fig. 4A and B). In addition, analyses of OCs that did form F-actin rings showed that 2-BP dose-dependently reduced the length of F-actin rings in these cells (Fig. 4C). Similarly, the average number of nuclei in mature OCs were remarkedly decreased in 2-BP-treated groups, compared to the vehicle-treated group (Fig. 4D). Thus, pharmacological inhibition of palmitoylation by 2-BP impaired F-actin ring formation *in vitro*. Next, we directly assessed the effect of 2-BP on bone-resorbing activity of OCs by *in vitro* resorption pit assays. As shown in Fig. 4E, 2-BP-treated groups exhibited significantly fewer and smaller resorbed pits, when compared to the vehicle-treated group. As a result, the portion of bone surface resorbed by OCs declined from 82 ± 3.4 in the control group to 46 ± 2.9, 23 ± 2.8, and 11 ± 1.1 in groups treated with 6.25 μM, 12.5 μM, and 25 μM 2-BP, respectively (Fig. 4F). Collectively, these results demonstrated that 2-BP suppressed RANKL-induced F-actin ring formation and osteoclastic bone resorption *in vitro*.

3.4. Pharmacological inhibition of palmitoylation mildly suppressed osteogenic differentiation of MC3T3-E1 cells

To investigate the role of palmitoylation in osteogenic differentiation, we then tested the effects of 2-BP on osteoblastic differentiation of MC3T3-E1 preosteoblasts. MC3T3-E1 cells were cultured in osteogenic medium with increasing concentrations of 2-BP for 7 days, and then subjected to ALP staining. As shown in Fig. 5A, the activity of ALP, an early marker of osteoblast differentiation, was strongly induced in MC3T3-E1 cells by osteogenic medium, which was minimally affected by 2-BP treatment. Consistently, ALP activity assay detected a robust induction of ALP activity in MC3T3-E1 cells by osteogenic medium, which was mildly suppressed by 25 μM 2-BP, but hardly affected by lower concentrations of 2-BP (Fig. 5B). Similarly, the mRNA levels of *Alpl* and *Runx2* in MC3T3-E1 cells were induced by osteogenic medium (Fig. 5C). This induction was moderately suppressed by 25 μM 2-BP, but not by lower concentrations of 2-BP (Fig. 5C). In addition, 2-BP also showed a dose-dependent inhibitory effect on the mRNA expression of *Sp7* and *Ibsp* (Fig. 5C). Thus, global inhibition of palmitoylation appeared to moderately suppress osteoblastic differentiation of MC3T3-E1 cells.

3.5. Inhibition of palmitoylation suppressed RANKL-induced expression of c-Fos and NFATc1 without affecting activation of major osteoclastic signaling pathways

To explore the potential mechanism of protein palmitoylation in regulating osteoclast differentiation and activity, we first performed western blot analysis to examine the effect of 2-BP on RANKL-induced activation of NF-κB, PI3K-AKT, and MAPK (including JNK, p38, and ERK) pathways, which are known to play key roles in osteoclast differentiation and activation. As shown in Fig. 6A, RANKL treatment rapidly induced phosphorylation of NF-κB, AKT, JNK, p38, and ERK in both vehicle- and 2-BP-treated BMMs. Quantitative analysis further confirmed that the phosphorylation levels of the above proteins were similar between vehicle-treated and 2-BP-treated BMMs at different time points (Fig. 6B), indicating that 2-BP had no significant effect on RANKL-induced activation of NF-κB, AKT and MAPK pathways. We then tested the impact of 2-BP on the expression of c-Fos and NFATc1, two essential osteoclastogenic transcriptional factors downstream of the RANKL-RANK signaling. Consistent with results from qPCR analysis that showed decreased mRNA expression of NFATc1 and c-Fos in 2-BP-treated BMMs, western blot further revealed that after 0, 1, 3 and 5 days of RANKL stimulation, the protein levels of NFATc1 and c-Fos in BMMs progressively increased (Fig. 6C and D). However, this induction was significantly blunted by 2-BP treatment (Fig. 6C and D). Collectively, these results suggest that pharmacological inhibition of protein palmitoylation suppresses osteoclastogenesis in part by attenuating c-Fos/NFATc1 expression.

3.6. Pharmacological inhibition of palmitoylation protected mice against ovariectomy-induced bone loss

The above *in vitro* experiments have revealed the critical role of palmitoylation in osteoclast differentiation. We next sought to evaluate the preventive effects of 2-BP on postmenopausal osteoporosis, a bone disease primarily caused by excessive bone resorption. To this end, we used the ovariectomized (OVX) mice as an animal model for postmenopausal osteoporosis in women. Specifically, C57BL/6 mice were subjected to OVX or Sham surgeries at 10 weeks of ages, and injected daily with vehicle or 2-BP starting at 3 days after surgery for 5 weeks. At the end of treatments, mice were sacrificed for analysis. As expected, OVX-operated mice exhibited complete loss of bilateral ovaries and marked uterine atrophy (Fig. 7A and B), confirming the successful establishment of the OVX model. The trabecular bones of the distal femur from these mice were then evaluated by μCT analysis. Three-dimensional (3D) μCT images revealed a dose-dependent protective effect of 2-BP against OVX-induced loss of femoral trabecular bone (Fig. 7C). Quantitative analyses further showed that OVX operations significantly increased the percentage of trabecular bone volume (BV/TV), trabecular bone number (Tb. N) and trabecular thickness (Tb. Th), and accordingly decreased trabecular separation (Tb.Sp) (Fig. 7D). However, these OVX-induced induction in BV/TV, Tb. Th and Tb.N were slightly rescued in the 2-BP-L group, but nearly completely reversed in the 2-BP-H group (Fig. 7D). In addition, a trend of dose-dependent decrease in Tb.Sp was also observed in 2-BP-treated groups, although these differences have no statistical significance (Fig. 7D). Consistent with the μCT results, hematoxylin and eosin (H&E) staining verified the protective effects of 2-BP on bone loss in OVX mice (Fig. 7E).

To further investigate whether 2-BP ameliorates OVX-induced bone

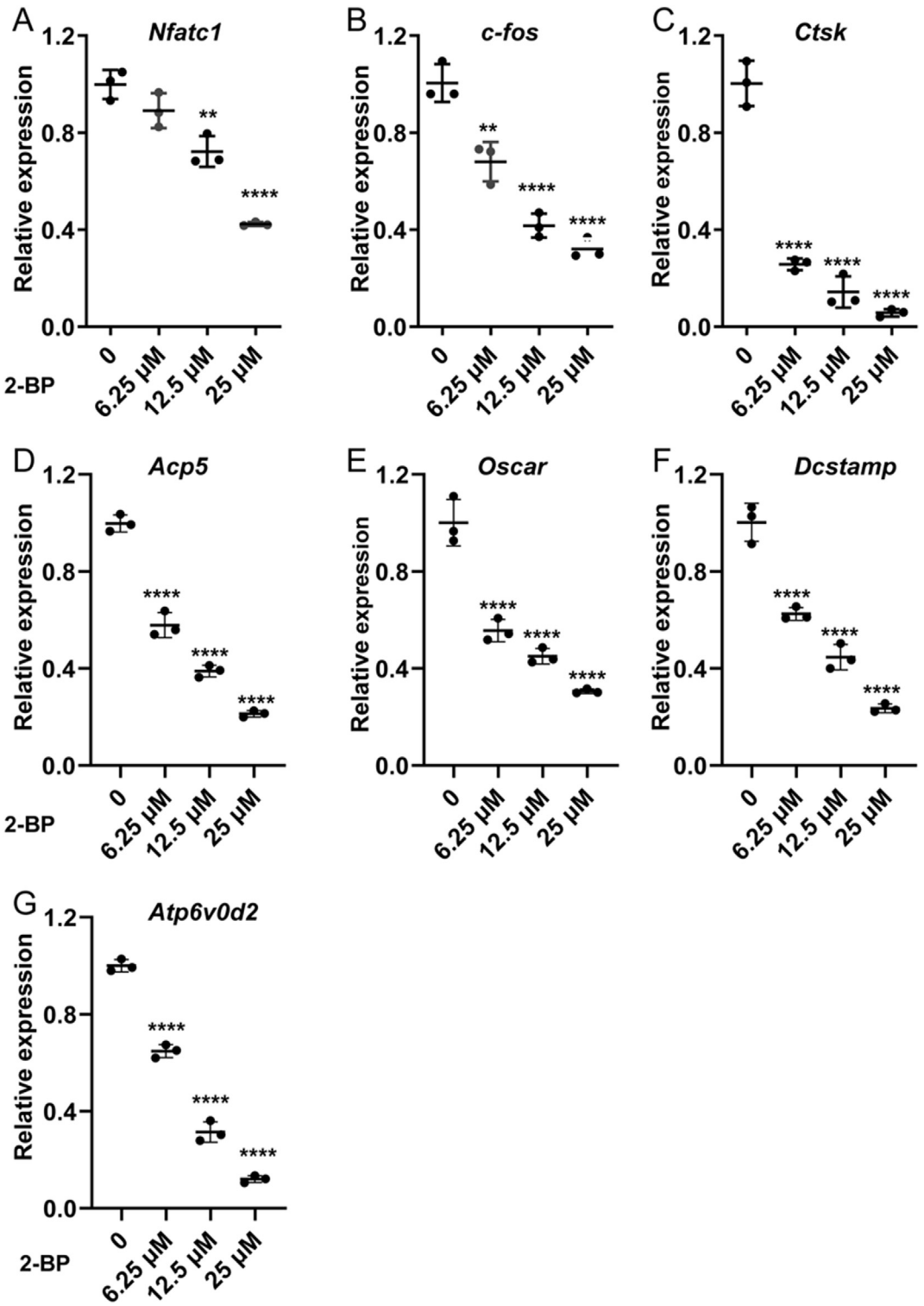

Fig. 3. 2-BP inhibited osteoclast-specific gene expression *in vitro*. qPCR analysis of relative expression of the osteoclast-specific genes *Nfatc1* **(A)**, *c-Fos* **(B)**, *Ctsk* **(C)**, *Acp5* **(D)**, *Oscar* **(E)**, *Dcstamp* **(F)**, and *Atp6v0d2* **(G)**, in BMMs treated with RANKL and different concentrations of 2-BP (0, 6.25, 12.5, or 25 μM) for 5 days. The relative changes in mRNA levels were analyzed by $2^{-\Delta\Delta CT}$ method. mRNA expression level of each target gene was first normalized to the expression of *18S* ribosomal RNA, and then normalized to the vehicle-treated group. All values were calculated from three biological replicates and presented as mean ± SD. *p* values were determined by one-way ANOVA. n = 3, *: $p < 0.05$, **: $p < 0.01$; ***: $p < 0.001$; ****: $p < 0.0001$, compared to vehicle-treated group.

loss by suppressing bone resorption *in vivo*, TRAP staining was performed on femoral sections, which revealed significantly increased number of TRAP + multinucleated OCs (N.Oc/BS) and the percentage of osteoclast surface relative to bone surface (Oc.S/BS) in OVX mice (Fig. 7F and G), confirming enhanced osteoclast formation and activity induced by OVX operations. However, these changes were dose-dependently inhibited by 2-BP treatment (Fig. 7F and G). Next, serum levels of type I collagen cross-linked C-terminal peptide (CTX-1) and osteocalcin (OCN), the commonly used markers of bone resorption and bone formation, respectively, were measured by ELISA assays. Indeed, compared with the

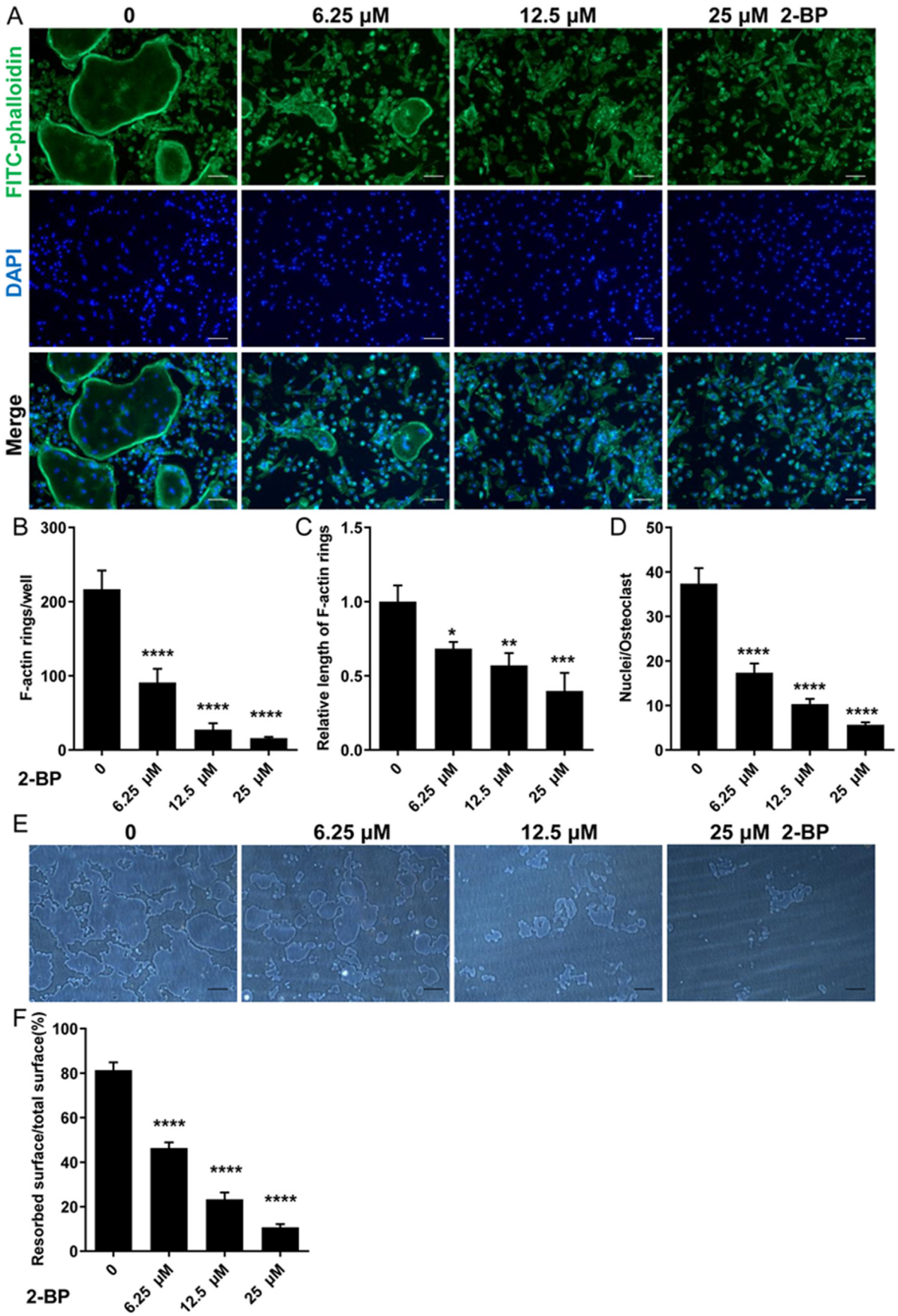

(caption on next page)

Fig. 4. 2-BP inhibited RANKL-induced F-actin ring formation and osteoclastic bone resorption *in vitro*. (A) Representative images of phalloidin staining of BMM cultures treated with RANKL and different concentrations of 2-BP (0, 6.25, 12.5, or 25 μM) for 5 days. F-actin rings. Green, F-actin; Blue, nuclei. Scale bar: 100 μm. **(B–D)** Quantification of average number of F-actin rings per well **(B)**, relative length of F-actin rings **(C)**, and average number of nuclei per osteoclast **(D). (E)** Representative images of resorption pits on the hydroxyapatite-coated surface of Corning Osteo Assay plate. Scale bar: 100 μm. **(F)** Quantification of the percentage of resorbed surface out of total surface on resorption pit images. All quantitative values were calculated from triplicates (n = 3) and presented as mean ± SD. p values were determined by one-way ANOVA. *: $p < 0.05$, **: $p < 0.01$; ***: $p < 0.001$; ****: $p < 0.0001$, compared to vehicle-treated group. (For interpretation of the references to colour in this figure legend, the reader is referred to the Web version of this article.)

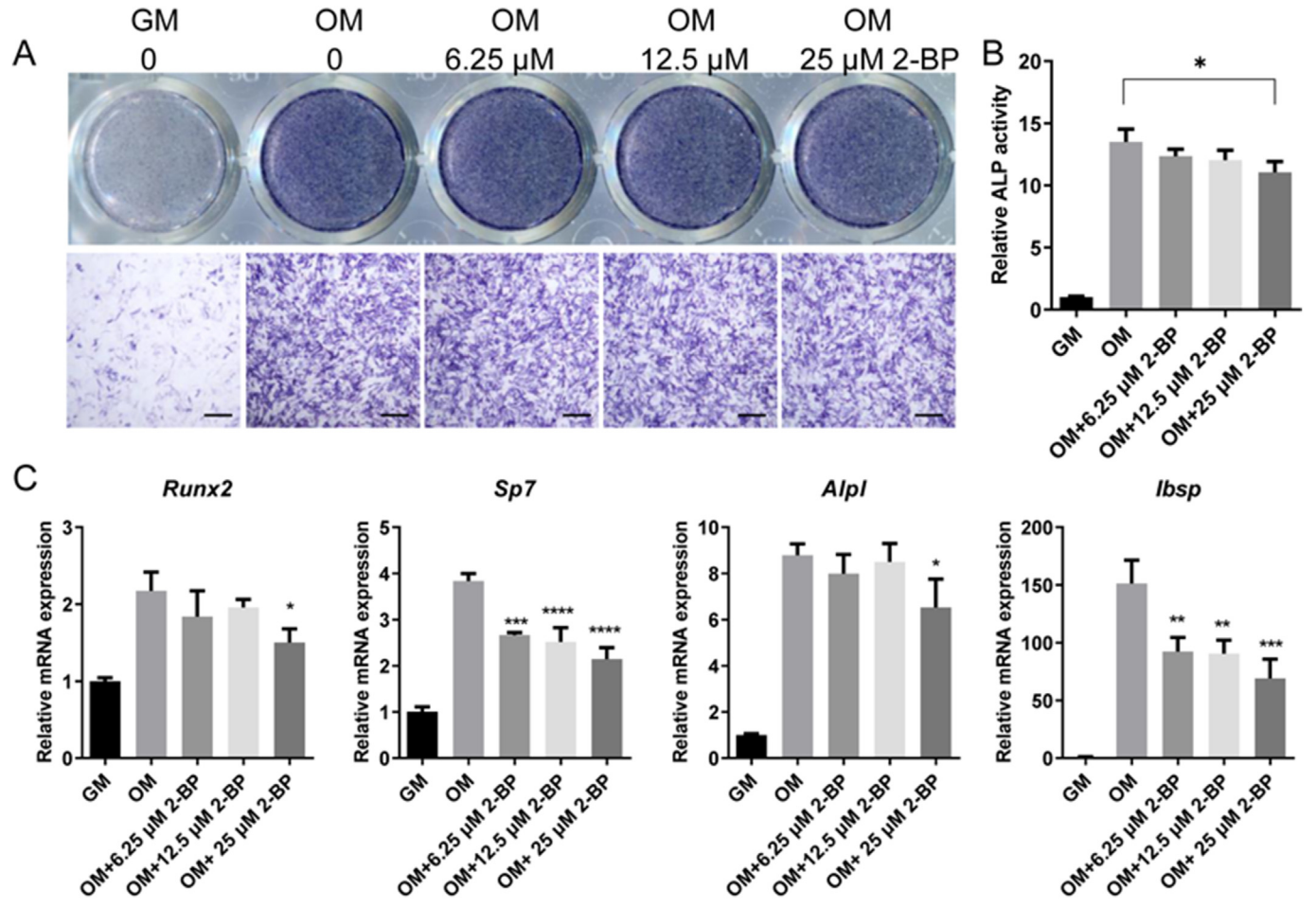

Fig. 5. Pharmacological inhibition of palmitoylation mildly suppressed osteogenic differentiation of MC3T3-E1 cells. (A) ALP staining of MC3T3-E1 cells after 7 days of treatment with growth medium (GM) or osteogenic medium (OM) in the presence of indicated concentrations of 2-BP. Images shown were representative results from triplicates. Scale bar: 400 μm. **(B)** ALP activity assay of MC3T3-E1 cells after 7 days of treatment with growth medium (GM) or osteogenic medium (OM) in the presence of indicated concentrations of 2-BP. n = 3. **(C)** qPCR analysis of relative mRNA expression of *Runx2*, *Sp7*, *Alpl*, and *Ibsp* in MC3T3-E1 cells after 7 days of treatment with growth medium (GM) or osteogenic medium (OM) in the presence of indicated concentrations of 2-BP. n = 3. All data were calculated from triplicates and presented as mean ± SD. p values were determined by one-way ANOVA. *: $p < 0.05$, **: $p < 0.01$; ***: $p < 0.001$; ****: $p < 0.0001$.

Sham group, serum CTX-1 levels were significantly increased in the OVX group but not in the 2-BP-H group (Fig. 7H), suggesting that 2-BP had a negative effect on bone resorption in OVX mice. On the other hand, serum OCN levels were significantly reduced upon OVX operation, which was partially reversed by treatment with 5 mg/kg 2-BP (Fig. 7I). Collectively, these results demonstrated that pharmacological inhibition of palmitoylation by 2-BP protected mice from OVX-induced bone loss by inhibiting osteoclastogenesis and bone resorption without impairing bone formation.

4. Discussion

Osteoclast-mediated bone resorption plays a central role in the pathogenesis of many bone diseases such as osteoporosis, osteoarthritis, rheumatoid arthritis, periodontal disease, periprosthetic osteolysis, and bone metastasis. Accordingly, a number of anti-resorption drugs, including bisphosphonates and denosumab, have been developed to treat these osteolytic diseases [22]. Unfortunately, these drugs have limited long-term benefits and cause some rare but serious side effects [22]. Therefore, the development of safer and more effective anti-resorption drugs remains an urgent task. The prerequisite for the identification of such novel anti-bone resorption targets is to elucidate the regulatory mechanisms of osteoclast differentiation and function. In this study, we reveal for the first time the critical role of palmitoylation in osteoclast differentiation and thus identify a promising therapeutic target for the treatment of osteolytic bone disease.

ZDHHC-mediated palmitoylation is a post-translational regulator of protein intracellular trafficking, subcellular localization, stability and activity as well as protein-protein interactions, and has been shown to regulate differentiation of multiple cell types [21,26–29]. However, it is unclear whether palmitoylation is involved in osteoclast differentiation and which ZDHHC is the key palmitoylation enzyme involved in this

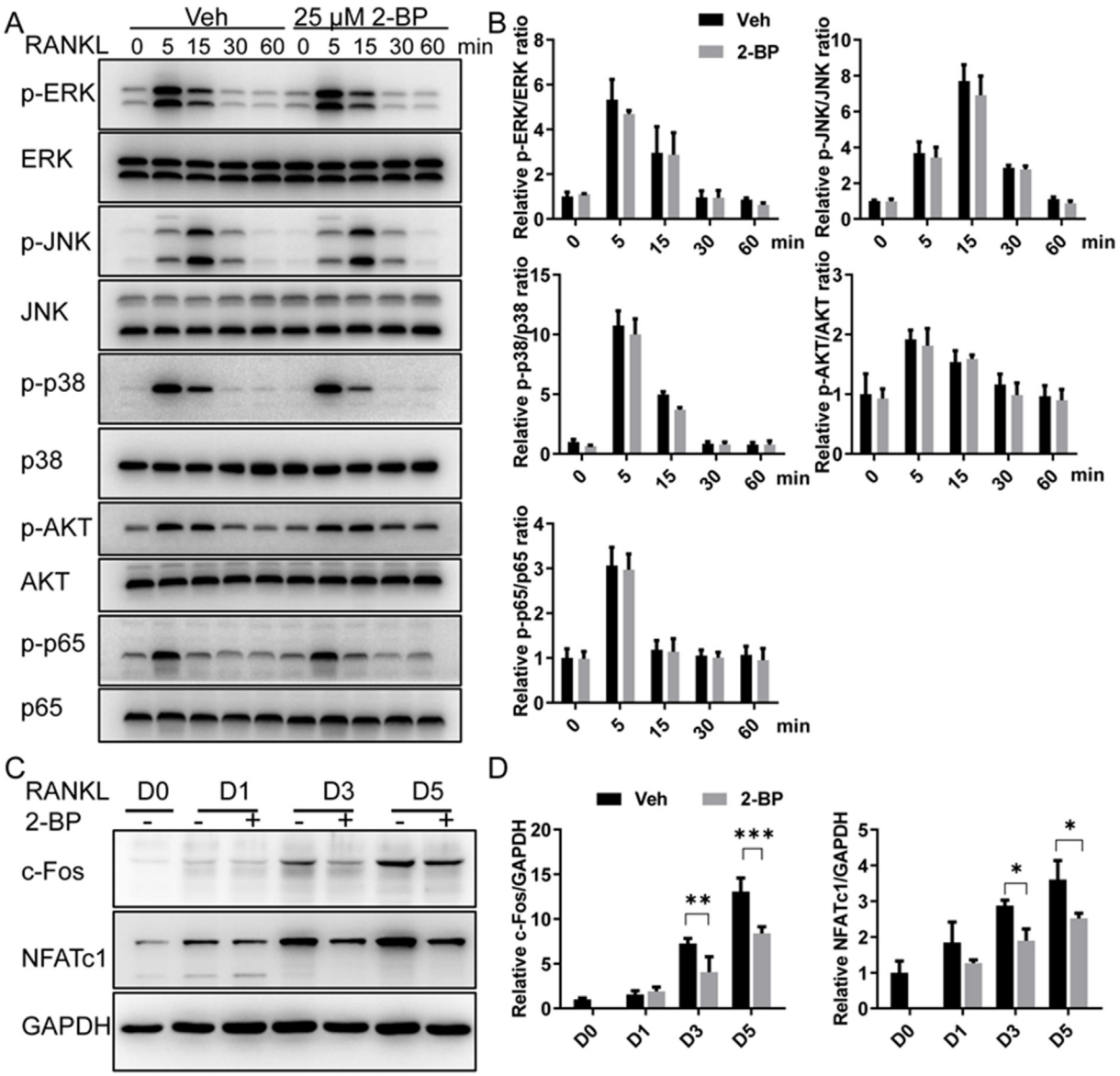

Fig. 6. Pharmacological inhibition of palmitoylation suppressed RANKL-induced expression of c-Fos and NFATc1 without affecting activation of major osteoclastic signaling pathways. (A) Western blot analyses of protein levels of phosphorylated ERK(p-ERK), total ERK, phosphorylated JNK (p-JNK), total JNK, phosphorylated p38 (p-p38), total p38, phosphorylated AKT (p-AKT), total AKT, phosphorylated NF-κB p65 (p-p65), and total NF-κB p65 (p65) in BMMs after stimulation with 100 ng/ml RANKL in the presence of vehicle (Veh) or 25 μM 2-BP (2-BP) for indicate times. Representative images from three independent biological replicates were shown. **(B)** Quantification of relative ratios of p-ERK/ERK, p-JNK/JNK, p-p38/p38, p-AKT/AKT, and p-p65/p65. n = 3 per group. **(C)** Western blot analyses of protein levels of NFATc1 and c-Fos in vehicle- or 25 μM 2-BP-treated BMMs at 0, 1, 3, and 5 days after RANKL stimulation. **(D)** Quantification of relative protein levels of NFATc1 and c-Fos in vehicle- or 25 μM 2-BP-treated BMMs at 0, 1, 3, and 5 days after RANKL stimulation. All data were calculated from triplicates (n = 3) and presented as mean ± SD. *p* values were determined by one-way ANOVA. *: $p < 0.05$, **: $p < 0.01$; ***: $p < 0.001$; ****: $p < 0.0001$.

process. In this study, we found that palmitoylation occurred in many proteins of differentiating OCs, and that pharmacological inhibition of palmitoylation by 2-BP inhibited RANKL-induced osteoclastogenesis *in vitro*, and prevented OVX-induced bone loss and bone resorption *in vivo*. These findings clearly demonstrated that palmitoylation plays a crucial role in osteoclast differentiation both *in vitro* and *in vivo*. Furthermore, we found that RANKL stimulation induced the mRNA expression of several *Zdhhc* genes, suggesting that these ZDHHCs may be key palmitoylation enzymes for osteoclast formation. Clearly, the specific role of these ZDHHCs in osteoclast formation and activity under physiological and pathological conditions remains to be determined. Despite these limitations, our results suggest that targeted inhibition of palmitoylation may be a promising therapeutic strategy for osteolytic bone disease.

NFATc1 and c-Fos are two master transcriptional regulators of osteoclast differentiation and function, and inactivation of either gene can lead to impaired osteoclast differentiation and severe osteosclerosis in mice [30,31]. During RANKL-induced osteoclastogenesis, c-Fos is induced by RANKL-RANK signaling, and subsequently binds to the promoter of *NFATc1* to stimulate its transcription. In this study, we showed that RANKL-induced expression of c-Fos and NFATc1 was significantly suppressed by 2-BP treatment, indicating that palmitoylation stimulates osteoclast formation by promoting the expression of c-Fos and NFATc1. While the molecular mechanism underlying this regulation is still unknown, several potential mechanisms warrant further investigation in the future. One possibility is that 2-BP may directly impair palmitoylation of c-Fos or NFATc1, thereby modulating their expression. Alternatively, 2-BP may act on the upstream regulator of c-Fos/NFATc1 to regulate their expression. Indeed, several signaling pathways, including

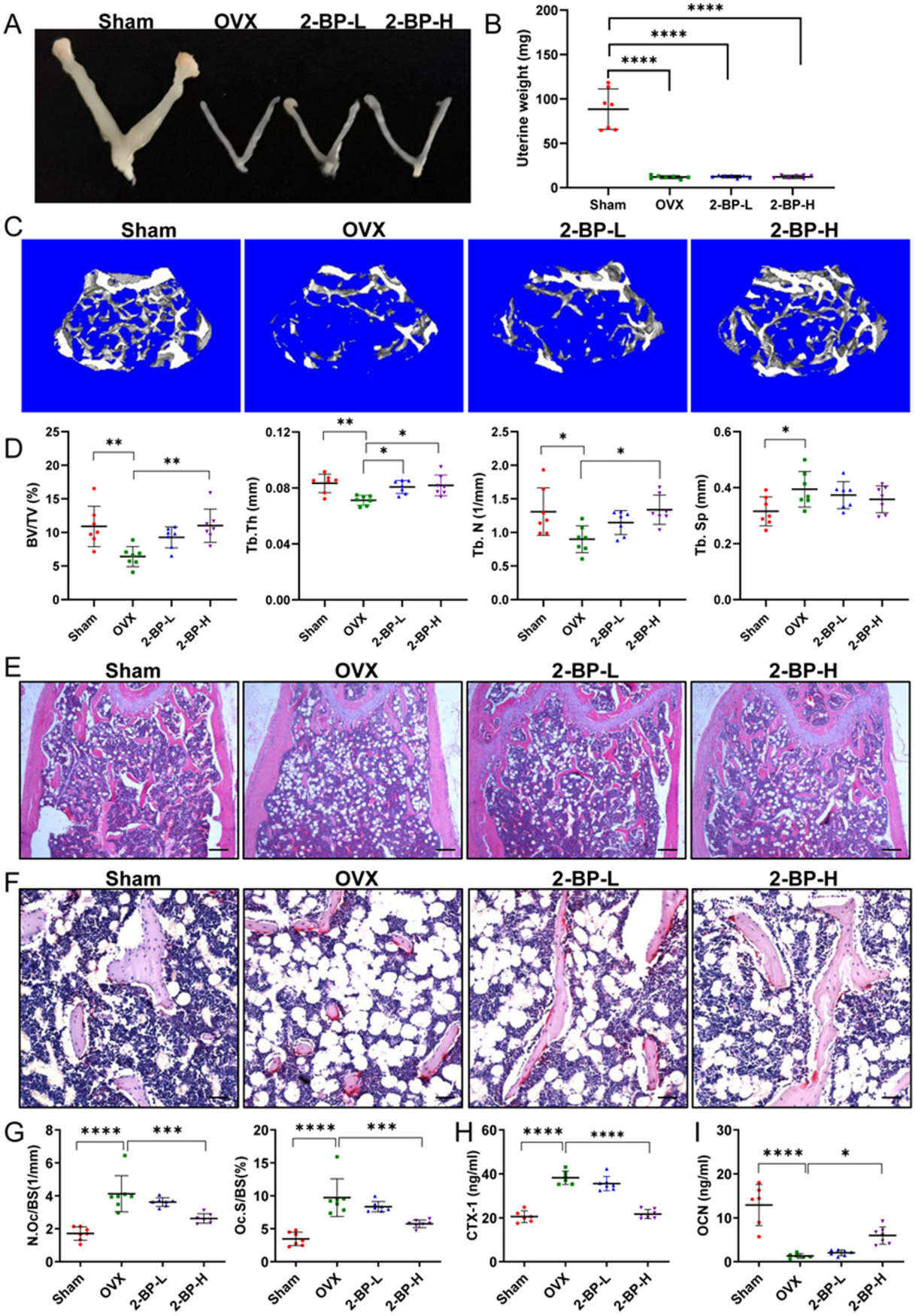

(caption on next page)

Fig. 7. Pharmacological inhibition of palmitoylation protected mice against ovariectomy-induced bone loss. (A–B) Gross morphology (A) and weights (B) of the uteri of Sham, OVX, 2-BP-L, and 2-BP-H mice. n = 7 mice for each group. **(C)** Representative three-dimensional μCT images of trabecular bones in the distal femurs from Sham, OVX, 2-BP-L, and 2-BP-H mice. **(D)** μCT analysis of the percentage of trabecular bone volume (BV/TV), trabecular number (Tb. N), trabecular thickness (Tb. Th), and trabecular separation (Tb. Sp) in the distal femurs. n = 7 mice for each group. **(E)** Representative images of H&E staining of the distal femurs from indicated mice. Scale bar: 200 μm. **(F)** Representative images of TRAP staining of the distal femurs from indicated mice. Scale bar: 50 μm. **(G)** Histomorphometry analysis of the images in F for number of OCs per trabecular bone surface (N. Oc/BS) and osteoclast surface per bone surface (Oc. S/BS). n = 7 mice for each group. **(H–I)** Serum levels of bone resorption marker CTX-1 (H) and bone formation marker OCN (I) were determined by ELISA analysis. CTX-1: type I collagen cross-linked C-terminal telopeptide. OCN: osteocalcin. n = 6–7 mice per group. All data were presented as dot plots with mean ± standard deviation. A single data point in the dot plot represents a value from a single mouse. *p* values were determined by one-way ANOVA with Tukey's post-hoc test. *: $p < 0.05$, **: $p < 0.01$; ***: $p < 0.001$; ****: $p < 0.0001$.

NF-κB, PI3K-AKT, and MAPK (JNK, p38, and ERK) pathways were known to function upstream of c-Fos/NFATc1. However, we did not observe any effect of 2-BP treatment on RANKL-induced activation of these signaling pathways, indicating that the action of palmitoylation on c-Fos and NFATc1 expression is not mediated by these osteoclastogenic pathways. Interestingly, two recent studies showed that STAT3 is the direct target of palmitoylation, whereas inhibition of palmitoylation impairs STAT3 phosphorylation and activation [27,28]. Moreover, pharmacological inhibition or osteoclast-specific deletion of STAT3 has been shown to suppress osteoclast differentiation and bone resorption [32,33]. Mechanistically, STAT3 was shown to regulate c-Fos expression or interact with c-Fos to promote NFATc1 transcription [32,33]. Therefore, 2-BP may suppress the expression of c-Fos and NFATc1 by inhibiting STAT3 palmitoylation and activation, thus inhibiting osteoclast differentiation. Similarly, palmitoylation was also shown to be critical for the methyltransferase activity of enhancer of zeste homologue 2 (EZH2), a histone methyltransferase essential for osteoclast differentiation and bone resorption, in glioma cells [34–36]. Therefore, it is possible that 2-BP might also be involved in the regulation of osteoclast differentiation via palmitoylation of EZH2. Clearly, further investigations were needed to elucidate the exact mechanism of palmitoylation in regulating osteoclast differentiation.

Previous studies have shown that many proteins are palmitoylated in differentiating OCs, and pharmacological inhibition of palmitoylation hindered osteoblast differentiation and mineralization in primary calvarial osteoblasts [18]. In line with these findings, our results showed that 2-BP mildly impaired osteogenic differentiation of MC3T3-E1 pre-osteoblasts. However, despite this suppressive effect of 2-BP on osteoblast differentiation *in vitro*, our animal experiments showed that 2-BP not only inhibited bone resorption, but also stimulated bone formation in OVX mice. One possibility is that our treatment approach resulted in a concentration of 2-BP *in vivo* sufficient to suppress osteoclast differentiation, but not the levels that impair osteoblast differentiation. Alternatively, 2-BP could indirectly promote osteoblast differentiation via osteoclast-osteoblast coupling. Consistent with this possibility, RANKL-induced osteoclastogenesis was found to be blocked at the TRAP + pre-osteoclast stage by 2-BP treatment. Since preosteoblasts have been shown to secrete PDGF-BB to stimulate angiogenesis [37], which is coupled with osteogenesis, inhibition of palmitoylation could indirectly promote osteogenesis through preosteoclast-induced angiogenesis.

In addition to OCs and osteoblasts, bone marrow microenvironment contains many other cell types, such as macrophages, bone lining cells, osteomacs, and vascular endothelial cells [38]. One limitation of this study is that we were unable to examine the effect of 2-BP on cell types other than osteoblast and OCs. However, recent studies have shown that protein S-palmitoylation can occur in macrophages and vascular endothelial cells [24,39,40]. In macrophages, palmitoylation of AKT is critical for its membrane attachment and subsequent phosphorylation, whereas inhibition of AKT palmitoylation attenuates proinflammatory activation in these cells [39]. Similarly, palmitoylation of endothelial nitric oxide synthase (eNOS) is essential for maintaining endothelial function by tethering eNOS to the plasma membrane of endothelial cells. Since macrophages and endothelial cells are important components of local bone microenvironment, the effects of 2-BP on bone metabolism may be mediated in part by interfering with S-palmitoylated proteins in these cells. Further studies are surely warranted to explore these possibilities.

In summary, our results showed that pharmacological inhibition of palmitoylation potently suppressed RANKL-mediated osteoclast differentiation *in vitro* and protected mice against OVX-induced osteoporosis *in vivo*. Our study also revealed that palmitoylation regulates osteoclast differentiation partly by promoting the expression of c-Fos and NFATc1. These findings not only revealed a novel role of palmitoylation in regulating osteoclast differentiation and bone resorption, but also provided a potential therapeutic target for the treatment of osteoporosis and other osteoclast-related diseases.

Ethics approval

All animal studies were performed under the National Institutes of Health (NIH) Guide for the Care and Use of Laboratory Animals, and approved by the Ethics Committee of Soochow University and the Experimental Animal Welfare Ethics Committee of Hangzhou City University.

Declaration of competing interest

All authors declare that they have no conflicts of interest.

Acknowledgements

This study was supported in part by the grants from the National Natural Science Foundation of China (81974344, 82272543) and Scientific Research Foundation of Hangzhou City University (No. J-202327).

Appendix A. Supplementary data

Supplementary data to this article can be found online at https://doi.org/10.1016/j.jot.2023.06.002.

References

[1] Lerner UH. Osteoclasts in Health and disease. Pediatr Endocrinol Rev 2019;17(2):84–99.
[2] Fornetti J, Welm AL, Stewart SA. Understanding the bone in cancer metastasis. J Bone Miner Res 2018;33(12):2099–113.
[3] Zhang L, Yang Y, Liao Z, Liu Q, Lei X, Li M, et al. Genetic and pharmacological activation of Hedgehog signaling inhibits osteoclastogenesis and attenuates titanium particle-induced osteolysis partly through suppressing the JNK/c-Fos-NFATc1 cascade. Theranostics 2020;10(15):6638–60.
[4] Wang S, Ma Q, Xie Z, Shen Y, Zheng B, Jiang C, et al. An antioxidant sesquiterpene inhibits osteoclastogenesis via blocking IPMK/TRAF6 and counteracts OVX-induced osteoporosis in mice. J Bone Miner Res 2021;36(9):1850–65.
[5] Zhu S, Zhu J, Zhen G, Hu Y, An S, Li Y, et al. Subchondral bone osteoclasts induce sensory innervation and osteoarthritis pain. J Clin Invest 2019;129(3):1076–93.
[6] Komatsu N, Takayanagi H. Mechanisms of joint destruction in rheumatoid arthritis - immune cell-fibroblast-bone interactions. Nat Rev Rheumatol 2022;18(7):415–29.
[7] Yang C, Tao H, Zhang H, Xia Y, Bai J, Ge G, et al. TET2 regulates osteoclastogenesis by modulating autophagy in OVX-induced bone loss. Autophagy 2022;18(12):2817–29.
[8] Chen K, Qiu P, Yuan Y, Zheng L, He J, Wang C, et al. Pseurotin A inhibits osteoclastogenesis and prevents ovariectomized-induced bone loss by suppressing reactive oxygen species. Theranostics 2019;9(6):1634–50.
[9] Kang H, Guo Q, Dong Y, Peng R, Song K, Wang J, et al. Inhibition of MAT2A suppresses osteoclastogenesis and prevents ovariectomy-induced bone loss. Faseb J 2022;36(2):e22167.

[10] Zhang Y, Qin Z, Sun W, Chu F, Zhou F. Function of protein S-palmitoylation in immunity and immune-related diseases. Front Immunol 2021;12:661202.
[11] Qu M, Zhou X, Wang X, Li H. Lipid-induced S-palmitoylation as a vital regulator of cell signaling and disease development. Int J Biol Sci 2021;17(15):4223–37.
[12] Jin J, Zhi X, Wang X, Meng D. Protein palmitoylation and its pathophysiological relevance. J Cell Physiol 2021;236(5):3220–33.
[13] Wild AR, Hogg PW, Flibotte S, Nasseri GG, Hollman RB, Abazari D, et al. Exploring the expression patterns of palmitoylating and de-palmitoylating enzymes in the mouse brain using the curated RNA-seq database BrainPalmSeq. Elife 2022:11.
[14] Liu Z, Xiao M, Mo Y, Wang H, Han Y, Zhao X, et al. Emerging roles of protein palmitoylation and its modifying enzymes in cancer cell signal transduction and cancer therapy. Int J Biol Sci 2022;18(8):3447–57.
[15] Wan J, Roth AF, Bailey AO, Davis NG. Palmitoylated proteins: purification and identification. Nat Protoc 2007;2(7):1573–84.
[16] Plain F, Howie J, Kennedy J, Brown E, Shattock MJ, Fraser NJ, et al. Control of protein palmitoylation by regulating substrate recruitment to a zDHHC-protein acyltransferase. Commun Biol 2020;3(1):411.
[17] Blanc M, David FPA, van der Goot FG. SwissPalm 2: protein S-palmitoylation database. Methods Mol Biol 2019;2009:203–14.
[18] Leong WF, Zhou T, Lim GL, Li B. Protein palmitoylation regulates osteoblast differentiation through BMP-induced osterix expression. PLoS One 2009;4(1): e4135.
[19] Song IW, Li WR, Chen LY, Shen LF, Liu KM, Yen JJ, et al. Palmitoyl acyltransferase, Zdhhc13, facilitates bone mass acquisition by regulating postnatal epiphyseal development and endochondral ossification: a mouse model. PLoS One 2014;9(3): e92194.
[20] Saleem AN, Chen YH, Baek HJ, Hsiao YW, Huang HW, Kao HJ, et al. Mice with alopecia, osteoporosis, and systemic amyloidosis due to mutation in Zdhhc13, a gene coding for palmitoyl acyltransferase. PLoS Genet 2010;6(6):e1000985.
[21] Li Z, Cheng Y, Jin X, Wang F, Wang X, Liu S, et al. ZDHHC16 restrains osteogenic differentiation of bone marrow mesenchymal stem cells by inhibiting phosphorylation of CREB. Heliyon 2023;9(1):e12788.
[22] Sun S, Xiu C, Chai L, Chen X, Zhang L, Liu Q, et al. HDAC inhibitor quisinostat prevents estrogen deficiency-induced bone loss by suppressing bone resorption and promoting bone formation in mice. Eur J Pharmacol 2022;927:175073.
[23] Lu Y, Yan JS, Xia L, Qin K, Yin QQ, Xu HT, et al. 2-Bromopalmitate targets retinoic acid receptor alpha and overcomes all-trans retinoic acid resistance of acute promyelocytic leukemia. Haematologica 2019;104(1):102–12.
[24] Wei X, Adak S, Zayed M, Yin L, Feng C, Speck SL, et al. Endothelial palmitoylation cycling coordinates vessel remodeling in peripheral artery disease. Circ Res 2020; 127(2):249–65.
[25] Baumgart F, Corral-Escariz M, Perez-Gil J, Rodriguez-Crespo I. Palmitoylation of R-Ras by human DHHC19, a palmitoyl transferase with a CaaX box. Biochim Biophys Acta 2010;1798(3):592–604.
[26] Wegleiter T, Buthey K, Gonzalez-Bohorquez D, Hruzova M, Bin Imtiaz MK, Abegg A, et al. Palmitoylation of BMPR1a regulates neural stem cell fate. Proc Natl Acad Sci U S A 2019;116(51):25688–96.
[27] Zhang M, Zhou L, Xu Y, Yang M, Xu Y, Komaniecki GP, et al. A STAT3 palmitoylation cycle promotes T(H)17 differentiation and colitis. Nature 2020; 586(7829):434–9.
[28] Ma Y, Liu H, Ou Z, Qi C, Xing R, Wang S, et al. DHHC5 facilitates oligodendrocyte development by palmitoylating and activating STAT3. Glia 2022;70(2):379–92.
[29] Zhang MM, Hang HC. Protein S-palmitoylation in cellular differentiation. Biochem Soc Trans 2017;45(1):275–85.
[30] Grigoriadis AE, Wang ZQ, Cecchini MG, Hofstetter W, Felix R, Fleisch HA, et al. c-Fos: a key regulator of osteoclast-macrophage lineage determination and bone remodeling. Science 1994;266(5184):443–8.
[31] Aliprantis AO, Ueki Y, Sulyanto R, Park A, Sigrist KS, Sharma SM, et al. NFATc1 in mice represses osteoprotegerin during osteoclastogenesis and dissociates systemic osteopenia from inflammation in cherubism. J Clin Invest 2008;118(11):3775–89.
[32] Yang Y, Chung MR, Zhou S, Gong X, Xu H, Hong Y, et al. STAT3 controls osteoclast differentiation and bone homeostasis by regulating NFATc1 transcription. J Biol Chem 2019;294(42):15395–407.
[33] Li CH, Xu LL, Jian LL, Yu RH, Zhao JX, Sun L, et al. Stattic inhibits RANKL-mediated osteoclastogenesis by suppressing activation of STAT3 and NF-kappaB pathways. Int Immunopharm 2018;58:136–44.
[34] Chen X, Ma H, Wang Z, Zhang S, Yang H, Fang Z. EZH2 palmitoylation mediated by ZDHHC5 in p53-mutant glioma drives malignant development and progression. Cancer Res 2017;77(18):4998–5010.
[35] Fan X, Gong M, Yu H, Yang H, Wang S, Wang R. Propofol enhances stem-like properties of glioma via GABA(A)R-dependent Src modulation of ZDHHC5-EZH2 palmitoylation mechanism. Stem Cell Res Ther 2022;13(1):398.
[36] Adamik J, Pulugulla SH, Zhang P, Sun Q, Lontos K, Macar DA, et al. EZH2 supports osteoclast differentiation and bone resorption via epigenetic and cytoplasmic targets. J Bone Miner Res 2020;35(1):181–95.
[37] Xie H, Cui Z, Wang L, Xia Z, Hu Y, Xian L, et al. PDGF-BB secreted by preosteoclasts induces angiogenesis during coupling with osteogenesis. Nat Med 2014;20(11): 1270–8.
[38] Kular J, Tickner J, Chim SM, Xu J. An overview of the regulation of bone remodelling at the cellular level. Clin Biochem 2012;45(12):863–73.
[39] Xiong W, Sun KY, Zhu Y, Zhang X, Zhou YH, Zou X. Metformin alleviates inflammation through suppressing FASN-dependent palmitoylation of Akt. Cell Death Dis 2021;12(10):934.
[40] Wei X, Schneider JG, Shenouda SM, Lee A, Towler DA, Chakravarthy MV, et al. De novo lipogenesis maintains vascular homeostasis through endothelial nitric-oxide synthase (eNOS) palmitoylation. J Biol Chem 2011;286(4):2933–45.